JOURNAL OF GEOPHYSICAL RESEARCH, VOL. 112, B11308, doi:10.1029/2006JB004802, 2007

Receiver function study of the crustal structure of the southeastern Caribbean plate boundary and Venezuela

Fenglin Niu,[1] Tammy Bravo,[2] Gary Pavlis,[2] Frank Vernon,[3] Herbert Rendon,[4] Maximiliano Bezada,[1] and Alan Levander[1]

Received 13 October 2006; revised 22 July 2007; accepted 31 August 2007; published 29 November 2007.

[1] We have investigated crustal thickness and composition across the southeastern Caribbean plate boundary with the receiver function technique. We used teleseismic data recorded by a temporary broadband array deployed under the BOLIVAR project and the permanent national seismic network of Venezuela. We used the primary P-to-S conversion and crustal reverberations to estimate crustal thickness and average crustal V_P/V_S ratio over the region. We observe large variations in crustal thickness and Poisson's ratio. Estimated Moho depth ranges from ~16 km beneath the southeastern Caribbean Sea to ~52 km beneath northeastern Venezuela and the Venezuelan Andes. There is a good correlation between crustal structure and tectonic terranes. Data from the Precambrian Guayana Shield suggest that the underlying crustal structure is relatively uniform with a moderate thickness (~37 km) and an intermediate composition. A thick crust is found below the foreland basins. The two mountain systems in northern Venezuela, the Serrania del Interior and the Serrania del Falcon, have a thin crust with arc composition and are likely dynamically supported by elastic rebound or underthrusting of the oceanic plateau that characterizes the southern Caribbean. On the other hand, the Venezuelan Andes and Perija Range on the western side of the country are probably isostatically balanced by thick crustal roots.

Citation: Niu, F., T. Bravo, G. Pavlis, F. Vernon, H. Rendon, M. Bezada, and A. Levander (2007), Receiver function study of the crustal structure of the southeastern Caribbean plate boundary and Venezuela, *J. Geophys. Res.*, *112*, B11308, doi:10.1029/2006JB004802.

1. Introduction

[2] The origin of continental crust has been a long term focus of the Earth sciences [*Taylor*, 1967; *de Wit et al.*, 1992]. It is now generally believed that the formation of the continents involved extensive collisional accretion of island arcs and microcontinental blocks although details of the aggregation are still unclear [*Hoffman*, 1988; *Nelson*, 1991; *Jordan*, 1988]. Since the bulk chemistry of modern island arcs and continental crust is quite different [*Taylor and White*, 1965; *Taylor and McLennan*, 1985; *Fountain and Christensen*, 1989; *Rudnick and Fountain*, 1995; *Christensen and Mooney*, 1995; *Suyehiro et al.*, 1996; *Holbrook et al.*, 1999], either chemical differentiation or mechanical refining processes have been involved in the arc accretion or different accretion processes have operated throughout geologic history to create the continents due to the evolving thermal history of the Earth. It is thus very important to identify age dependencies in crustal structure and composition.

[3] *Durrheim and Mooney* [1994] argued for a substantial difference between Archean and Proterozoic crust in both thickness and composition. They found that Proterozoic terranes are characterized by a several-km-thick lowermost mafic layer, which is not typically seen beneath Archean terranes. Mixed observations have been reported regarding whether such a characteristic difference exists or not. *Nguuri et al.* [2001] and *Niu and James* [2002] found that the crust beneath the Kaapvaal and Zimbabwe cratons is relatively thin (~35 km). The Moho-discontinuity is extremely flat and sharp with a large velocity and density contrast which indicates the lack of a high velocity mafic layer in the lower crust. Contradictory observations, however, have also been reported. For example, a global study of average crustal V_P/V_S ratio by *Zandt and Ammon* [1995] favors the presence of a mafic layer beneath cratons. The Deep Probe experiment [*Henstock et al.*, 1998; *Snelson et al.*, 1998] identified a very thick (~25 km) mafic layer at the base of the Archean Wyoming province. A comparison between Archean and Proterozoic globally is very important to the understanding of continental formation and evolution in the early stage as well as Precambrian global tectonics.

[4] The present study is part of the passive seismic experiment under the BOLIVAR (Broadband Ocean-Land Investigations of Venezuela and the Antilles arc Region) and GEODINOS (Geodinámica Reciente del Límite Norte de la Placa Sudamericana–Recent Geodynamics of the

[1]Department of Earth Science, Rice University, Houston, Texas, USA.
[2]Department of Geological Sciences, Indiana University, USA.
[3]Scripps Institution of Oceanography, University of California, USA.
[4]FUNVISIS, El Llanito, Venezuela.

0148-0227/07/2006JB004802$09.00

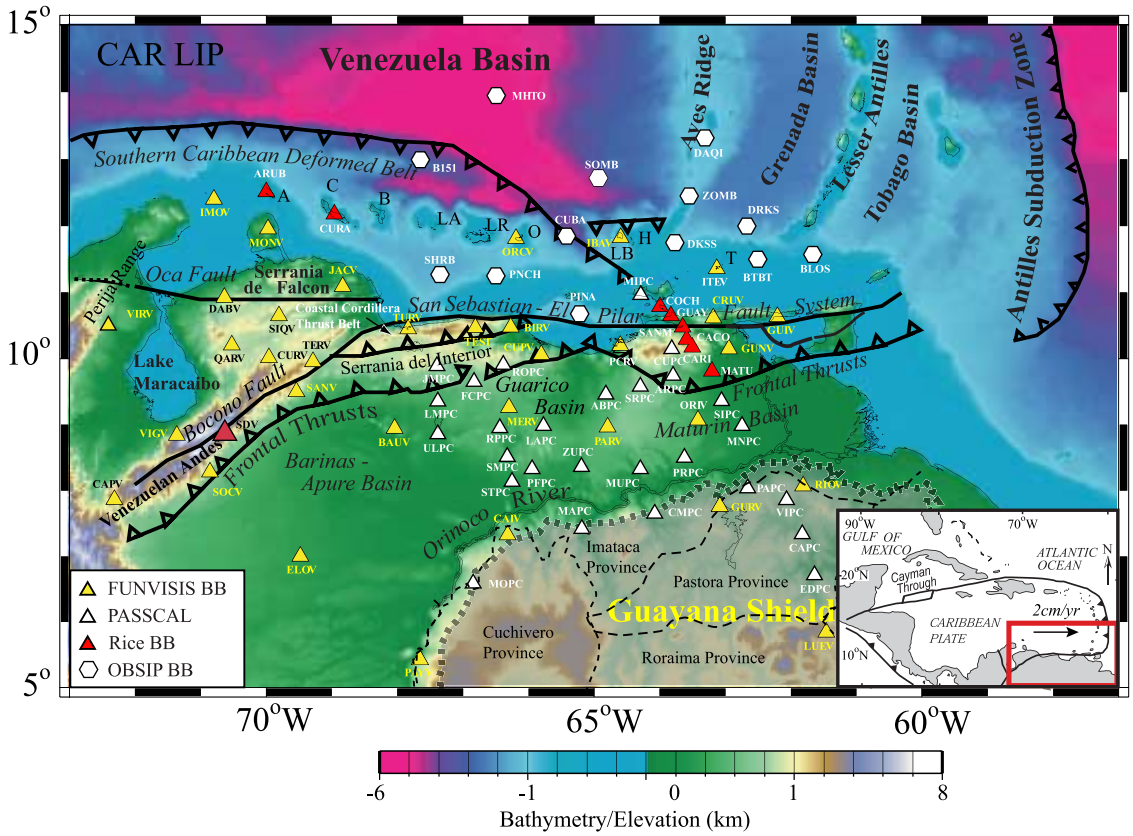

Figure 1. Location map showing the BOLIVAR and GEODINOS study area, principal plate boundary fault systems, and BOLIVAR passive seismic experiment. Triangles and Hexagons indicate the land and ocean floor broadband stations, respectively. Islands of the Leeward Antilles Archipelago: A = Aruba, C = Curaçao, B = Bonaire, LA = Las Aves, LR = Los Roques, O = Orchilla, LB = La Blanquilla, T = Testigos. Inset shows the Caribbean plate and surrounding area and arrow indicates its present motion direction with respect to stable South America. Large red triangle in western Venezuela is the IRIS GSN station SDV.

Northern Limit of the South American Plate) projects. These projects aimed to study island arc accretion processes occurring at the northern margin of South America with geological, geochemical and seismic structure investigations of the Caribbean and South America plate boundary zone and the surrounding area [*Levander et al.*, 2006]. As a result the focus of this study is Venezuela, its northern continental margin, and the southern Caribbean.

[5] The northern margin of South America originated in late Triassic time when the supercontinent Pangaea broke up and the North and South Americas drifted apart [see *Ostos et al.*, 2005 for a review]. From the Paleocene to the present, the margin appears to have experienced oblique collision with the Caribbean plate progressively from west to east as the Americas moved westward past the Caribbean and converged slightly [*Burke*, 1988], although the extent that collision drove the tectonics is open to debate. The oblique collision created a broad and complicated diffuse Caribbean-South America plate boundary zone containing strike-slip, compressional and extensional structures [*Gordon*, 1998] (Figure 1). This also resulted in spatial and temporal juxtaposition of former island arc structures on the Caribbean plate with the evolving of fold and thrust belts and foreland basins onshore, including the Coastal Cordillera Thrust Belt. The formation of the foreland basins is often attributed to the flexure loading of the lithosphere by the overthrust belts. Geodynamic modeling of *Jacome et al.* [2002] however, suggested that the Maturin basin subsidence actually has two primary contributors: thrust sheet loading and continental subduction. Knowledge of the lithospheric structure such as variations in the thickness of the crust and mantle lid is thus an important constraint on any tectonic models for this region.

[6] Previous seismic studies of the crustal structure and Moho depths in Venezuela are limited. A few active source experiments have been conducted in eastern Venezuela. *Schmitz et al.* [2002, 2005] found that the crust thickness beneath the Precambrian Guayana Shield is about 45 km and it decreases to about 35 km near the coast. Because of the difficulty in generating and recording shear waves, the great majority of active source seismic surveys have used compressional wave information to derive velocity models of the crust. Ideally both the P- and S-wave velocities are desired to infer the crustal composition. Here we apply the receiver function technique to estimate Moho depth and average crustal V_P/V_S ratio using the data recorded by the 83 broadband stations deployed under the BOLIVAR and GEODINOS projects. The stations provide a fairly uniform sampling of a large part of northern Venezuela and the southern Caribbean, covering a wide range of tectonic provinces.

Our main goal is to present a crustal thickness model of the area as constraint for ongoing geological and geodynamical studies. An accurate crustal model is also essential to determine the deep lithosphere and mantle structures. We also address the issue of whether the Precambrian Guayana Shield has a distinct seismic structure and composition similar to observations made on other continents [*Durrheim and Mooney*, 1994; *Nguuri et al.*, 2001; *Niu and James*, 2002; *Henstock et al.*, 1998]. This is of interest as this is the first time widespread crustal thickness measurements have been made on the Guayana Shield.

2. Receiver Function Analysis

[7] The teleseismic P coda is composed of S waves converted from P at various depths below the station. The coda thus contains considerable information about the structure directly beneath the station. The receiver function technique is designed to isolate these P to S conversions [*Langston*, 1979; *Owens et al.*, 1984] by deconvolution of a vertical (or longitudinal) component from a radial (or in-plane transverse) component in either the time domain or frequency domain [*Ammon*, 1991; *Gurrola et al.*, 1995; *Niu and Kawakatsu*, 1996; *Dueker and Sheehan*, 1998; *Park and Levin*, 2000; *Sheehan et al.*, 2000; *Poppeliers and Pavlis*, 2003]. Substantial artifacts may be introduced in the deconvolution when noise levels are high. A straightforward frequency domain spectral division can be extremely unstable due to spectral holes in the vertical-component spectrum. To stabilize the deconvolution either a "prewhitening" [*Yilmaz*, 2001] or a "water-level" [*Clayton and Wiggins*, 1976; *Ammon*, 1991] technique is used. The former adds a small component of random noise to the vertical component, while the later sets a lower bound on its magnitude.

[8] As the P to S converted wave from the Moho is the dominant phase seen on the receiver functions, early receiver function studies mainly used this primary conversion phase to determine the Moho depth with an assumed velocity model. With adequate distance coverage in the data, one can use velocity analysis to determine the optimum depth of a discontinuity and the average velocity above it [*Gurrola et al.*, 1994; *Niu and Kawakatsu*, 1998].

[9] Besides the P to S conversion, a receiver function also contains other coherent signals, such as the Moho reverberation phases, which are the multiple reflections from the free surface and the Moho. Recent receiver function studies have shown that one can estimate the average crustal V_P/V_S ratio together with a better determined Moho depth with the arrival times of the conversion and the reverberation phases [*Zandt and Ammon*, 1995; *Zhu and Kanamori*, 2000; *Niu and James*, 2002]. The crustal V_P/V_S ratio provides additional information that can help constrain the bulk composition of the continental crust. *Niu and James* [2002] observed very strong crustal multiples from the Kimberley Array deployed in the Kaapvaal craton, South Africa. They used the amplitude information to determine both the velocity and density jump across the Moho.

3. BOLIVAR Passive Seismic Observations

[10] The passive seismic data collected under the BOLIVAR project includes: (1) an ~18-month deployment (November 2003–May 2005) of 27 PASSCAL broadband seismographs from the IRIS PASSCAL facility; (2) a ~12-month deployment (February 2004–February 2005) of 13 OBSIP (The US National Ocean Bottom Seismograph Instrument Pool) broadband instruments; and (3) an ongoing deployment of 8 Rice broadband seismometers since November, 2004. In addition, shortly before the temporary stations were deployed the Venezuelan government finished an upgrade of their seismic network from short-period analog to broadband digital recording. The new national network run by FUNVISIS (Venezuelan Foundation for Seismological Research), consists of 34 satellite-telemetered broadband stations. At the peak deployment, with the FUNVISIS, PASSCAL, OBSIP and Rice instruments and 1 GSN (Global Seismic Network) station in the area, we were recording data at 83 stations (Figure 1).

[11] The 83 stations formed a large 2D areal array with an aperture ~1200 km from east to west and ~600 km from north to south. For the remainder of this paper, we will refer to these stations as the BOLIVAR array. Station spacing varies from ~10 km in a highly dense line near 64° west to ~100 km in western Venezuela, which is covered mainly by the FUNVISIS network. The station spacing in the west is too coarse to use modern array techniques, such as common-conversion-point gathering and pre-stack depth migration, to image the crustal structural [*Levander*, 2003]. Thus the classic single station stacking technique is employed here to extract the crustal structure around stations.

4. Data Selection and Analysis

[12] **Event selection**. We have analyzed seismograms from 313 earthquakes with magnitude $Mw \geq 5.0$ and in the epicentral distance range of 30°–90°. From these we have chosen 112 earthquakes with the best signal-to-noise ratio (SNR). These earthquakes provide a reasonably good distance and azimuth coverage (Figure 2).

[13] We first rotated the two horizontal components of the seismograms to the radial and transverse components. The direct P wave is normally the dominant energy in the radial component and in the subsequent receiver function formed from it. The direct P wave could interfere with P to S conversions generated at shallow depths, such as at the base of a sediment layer. To minimize the P wave energy in the receiver function, we project the two components to the principle directions (longitudinal and in-plane transverse) computed from the covariance matrix. The receiver functions are then computed from the data projected into this coordinate system (hereafter referred as to P- and SV-component) [*Niu and Kawakatsu*, 1998; *Vinnik*, 1977; *Reading et al.*, 2003; *Niu et al.*, 2004].

[14] **Deconvolution**. We employed the "water-level" deconvolution technique [*Clayton and Wiggins*, 1976; *Ammon*, 1991] to generate receiver functions:

$$RF(\omega) = \frac{V(\omega)P^*(\omega)}{\max\left\{P(\omega)P^*(\omega),\ k|P_{\max}(\omega_0)|^2\right\}} e^{-\left(\frac{\omega}{2a}\right)^2}. \quad (1)$$

[15] Here k is the "water-level", which is set to 0.03. $P(\omega)$ and $V(\omega)$ are the spectra taken from a 40 s time window (5 s before and 35 s after the P) of the P- and SV-

Figure 2. Locations of the 112 teleseismic events used in this study. Open circles indicate earthquakes located at depths that are shallower than 50 km and diamonds indicate earthquakes occurring at depths greater than 50 km.

components. The width factor, a, of the Gaussian lower-pass filter was set to 1.5. We used a bandpass filter of 0.01–2 Hz for the PASSCAL and RICE stations (STS2 and CMG3T) and 0.02–2 Hz for the FUNVISIS stations (CMG-40T) before the deconvolution.

[16] **Orientation estimates of the OBS stations**. For the OBSIP stations, we determined the azimuths, θ_1 and θ_2, of the two horizontal components (BH1, BH2) using teleseismic P waves with high SNR. Note the instruments constrain $\theta_2 = \theta_1 + 90°$. The azimuths were chosen when the summed P wave energy in the transverse component reaches its minimum. For an assumed azimuth, θ_1, which is defined clockwise from north, we first rotated horizontal seismograms to radial and transverse directions based on raypath geometry. We then computed the weighted summation of the transverse P wave energy for all events. The total number of events used for each station is between 24 and 26. The weight was calculated from the product of SNR and linearity of the P wave particle motion. θ_1 was taken in the range of 0° to 180° with an increment of 1°. There are two possible azimuths, θ_1 and $\theta_1 + 180°$, in which the transverse component reaches the minimum. Finally, we took the cross correlation (cc) between the vertical and radial components and chose the azimuth that shows a positive correlation. In general, this worked very well. The 180° ambiguity, however, remains when the correlation between the vertical and horizontal is lower. The measured θ_1 and their standard deviations are shown in Table 1. We used the same approach to confirm the orientations of the land stations. The estimated orientations of the north–south component are in the range of −38° to 26° with an average of −5 ± 9°. We note that this accuracy is sufficient for the purpose for which we are using these data. That is, as long as the alignment is good enough to allow a deconvolution of converted phases with the right polarity and approximately correct amplitude the results can be used to estimate crustal thickness and V_P/V_S ratio.

[17] **Velocity Models**. To convert traveltimes to depths, we used velocity models derived from refraction and reflection/wide-angle seismic data [*Schmitz et al.*, 2002, 2005; S. A. Clark et al., Characterizing the diffuse plate boundary between the Caribbean and South American Plates at 64°W, submitted to *Journal of Geophysical*

Table 1. OBS Station Orientation

Station	Lat., °	Lon., °	Elevation, km	BH1cmpaz, [a]
B151	12.9915	−67.6513	−3.616	−96 ± 15
BLOS	11.5708	−61.6677	−0.461	82 ± 14
BTBT	11.4989	−62.5010	−0.129	–
CUBA	11.8499	−65.4180	−3.997	154 ± 13
DKSS	11.7515	−63.7699	−1.117	−152 ± 23
DRKS	11.9992	−62.6685	−2.400	−122 ± 03
MHTO	13.9497	−66.4910	−4.997	−69 ± 03
PINA	10.6796	−65.2200	−1.103	−76 ± 10
PNCH	11.2493	−66.5009	−0.908	176 ± 28
SHRB	11.2707	−67.3496	−1.860	115 ± 06
SOMB	12.7209	−64.9313	−3.853	−134 ± 14
ZOMB	12.4511	−63.5522	−0.644	−68 ± 27

[a]Orientation of BH1 defined as clockwise from north, BH2 is oriented 90° clockwise from BH1.

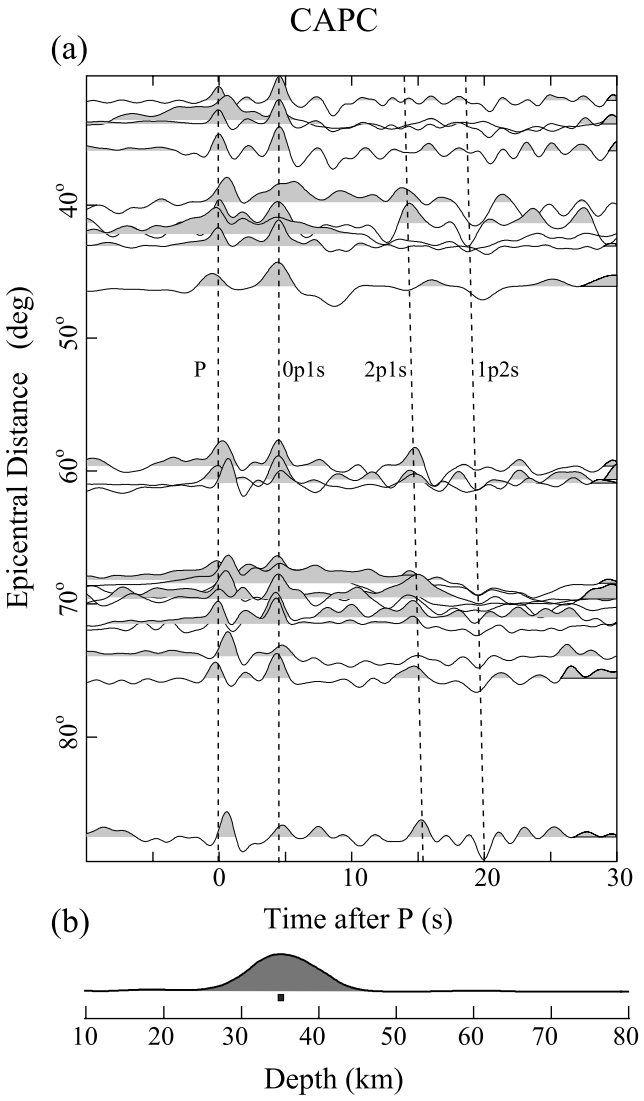

Figure 3. (a) An example of the individual receiver functions recorded at station CAPC. The receiver functions are generated from the radial and vertical components. Dashed line indicates the arrival times of the primary P to S conversion phase, 0p1s, and the two Moho reverberation phases, 2p1s and 1p2s. Following *Niu and James* [2002], we used the notation of *npms*, where *n* and *m* are the numbers of P- and S-wave legs within the crust, respectively, to refer the P to S conversion phase and the Moho reverberation phases. (b) The stacked receiver function after time-to-depth conversion. Note the prominent P to S conversion as well as the two reverberation phases in (a) and the remarkably clear peak in (b). Square dot indicates the Moho depth. Depth is corrected from the sea level and a 4th-root stack is applied here.

Research, 2007; M. B. Magni et al., Crustal structure of the South American-Caribbean plate boundary at 67.5 W from controlled-source seismic data, submitted to *Journal of Geophysical Research*, 2007; *Guédez et al.*, 2006; *Guédez*, 2007; *Bezada et al., unpublished*]. For stations located within 50 km of an active source line, we constructed a 1D P wave velocity model by projecting the refraction model to the station. Locations of the active source profiles are shown in Figure 5. For those stations that are >50 km away from any active source profiles, we used crustal 5.1 [*Mooney et al.*, 1998] to form a 1D reference velocity model. Where V_P/V_S measurements are available from analysis of multiple reflections in the receiver functions, we used them to construct 1D S-wave velocity models for the depth stacking. Otherwise we used a default V_P/V_S = 1.732.

[18] **Depth Stacking**. We manually checked all the seismograms and chose the receiver functions whose vertical components after deconvolution have a well defined simple pulse at time zero. The number of selected receiver functions ranged from 4 to 78 depending on the site condition and the recording history of a station. As an example, in Figure 3a we show the individual receiver functions recorded at station CAPC.

[19] To determine Moho depth beneath a station, we assumed that the Moho is relatively flat and stacked the receiver functions gathered at each station. Stacking was performed in the depth domain. For a conversion depth d, we first calculated the raypath of converted phase *Pds* and its arrival time (τ_d) relative to P by ray tracing the 1D P- and S-wave velocity model discussed above. We then summed the N seismograms within a 0.1 s window centered on the arrival time of *Pds* using an nth-root stacking technique [*Muirhead*, 1968; *Kanasewich*, 1973]. Let x_j (t) represent the jth receiver function recorded at a station, and τ_{dj} is the *Pds* arrival time for a Moho with a depth of d, an nth-root stack, $y(d)$, is given by

$$y(d) = r(d)|r(d)|^{N-1}, \tag{2}$$

where

$$r(d) = \frac{1}{K}\sum_{j=1}^{K} sign\left(x_j(\tau_{dj})\right)|x_j(\tau_{dj})|^{1/N} \tag{3}$$

[20] Here K is the total event number recorded at the station. We chose $n = 4$ to reduce the uncorrelated noise relative to the usual linear stack ($n = 1$). We varied d from 0 to 100 km in an increment of 1 km. An example of the depth stacked receiver function is shown in Figure 3b.

[21] **V_P/V_S Ratio Estimation**. Some stations showed prominent reverberation signals in the stacked receiver functions (Figure 4a). We used arrival times of 0p1s, 2p1s and 1p2s to constrain the average crustal V_P/V_S ratio. To do this, we first used the 1D P wave velocity as discussed above to calculate the S-wave velocity based on the assumed V_P/V_S ratio. The ratio is varied in the range of 1.5 to 2 with an increment of 0.001 for land stations and 1.5 to 2.5 for OBS stations. For each V_S, we then performed the time to depth conversion by assuming three different modes: the primary P to S conversion 0p1s mode, the reverberation 1p2s and 2p1s modes. The time to depth conversion was performed in the range of 0 to 100 km with an increment of 1 km. The three depth traces were then summed with different weights. We further used the cross correlations

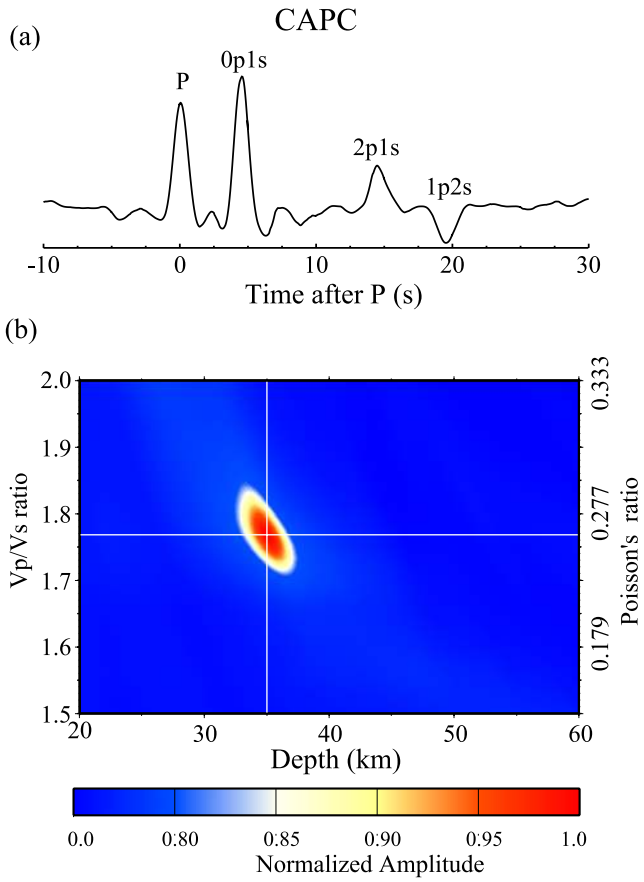

Figure 4. (a) Receiver functions generated from the SV- and P-components recorded at station CAPC are stacked in the time domain. Moveout of each trace is calculated based on a relative slowness of −0.005 s/deg with respect to the P wave. (b) Color contour of the summed amplitude as a function of crustal thickness and V_P/V_S ratio. Location of the amplitude peak is indicated by the two white lines.

between the three modes as a weight function and summed the three depth traces:

$$A(d,r) = \frac{c(r)}{w_1 + w_2 + w_3} \cdot \left[w_1 A_{op1s}(d,r) + w_2 A_{2p1s}(d,r) + w_3 A_{1p2s}(d,r)\right]. \quad (4)$$

[22] Here d and r are the Moho depth and V_P/V_S ratio. w_1, w_2 and w_3, are the weights for 0p1s, 2p1s and 1p2s and $c(r)$ is the cross correlation weight. The weights assigned to the three modes were w_1 = 0.50, w_2 = 0.25 and w_3 = 0.25. Moho depth and V_P/V_S ratio were determined where the summed amplitude reaches its maximum. We also used three different combinations: (1) all three modes, (2) 0p1s and 1p2s modes, and (3) 0p1s and 2p1s modes to search the maximum. We accept those measurements only when two or all of them have consistent results. An example of the V_P/V_S ratio measurement is shown in Figure 4b.

5. Results and Discussion

[23] We obtained a total of 63 Moho depths and 34 V_P/V_S ratio measurements from the 83 stations. The results are listed in Table 2. The table is organized by grouping stations in the following tectonic/physiographic regions: the Guayana Shield, the foreland basins, coastal plains, Serrania del Interior, Serrania del Falcon, Venezuelan Andes, ocean islands, and southeast Caribbean Sea. 1σ errors are calculated based on a bootstrap method [*Efron and Tibshirani*, 1986], but we note that these are formal errors, that do not include uncertainty in the velocity model, and actual errors are likely higher.

[24] For those stations at which we were not able to identify the Moho, about half are OBS and island stations where very few receiver functions were available because of high noise levels or a very short recording period. The other half are stations deployed in the foreland basins. They have recorded very strong sediment induced reverberations, making it hard to pick the P to S converted wave from the Moho.

[25] The Moho relief map based on the 63 measurements is shown in Figure 5a. The interpolation was performed to fit a flattest Moho. An inversion algorithm was employed in the interpolation. We divided the study area between 73°W to 60°W and 5°N to 14°N into meshed grids of 0.25° × 0.25°. Moho depths at grid nodes, m_{ij}, are considered as unknown parameters (total 53 × 27 = 1961). The 63 observations, d_n, were then projected to the nearest grid nodes. **G** is the kernel matrix with a dimension of 63 × 1961. It has 63 none zero elements (=1) that corresponds to the 63 observations. This gives a total of N = 63 equations:

$$\mathbf{Gm} = \mathbf{d} \quad (5)$$

[26] To solve the equation (5) we also added the regularization that minimizes the first derivative of the model (flattest Moho, first-order Tikhonov regularization) [*Aster et al.*, 2004]:

$$\mathbf{Lm} = \mathbf{0}, \quad (6)$$

Here **L** is the finite difference operator matrix of the first derivative in a 2 dimensional problem. Combining equations (5) and (6) we solved the damped least squares problem to minimize the objective function:

$$\| \mathbf{Gm} - \mathbf{d} \|^2 + \lambda^2 \| \mathbf{Lm} \|^2 . \quad (7)$$

Here λ is a regularization parameter, and is selected to meet the condition that the chi-square defined below equals to one.

$$\chi^2 = \sum_{i=1}^{N} \frac{\left(d_i - (\mathbf{Gm})_i\right)^2}{\sigma_i^2} \quad (8)$$

Here σ_i is the uncertainty in each measurement.

[27] The resulting Moho relief map shows a highly variable crustal structure. The estimated Moho depths range from 16 km beneath the Bonaire Basin to ~53 km beneath northeastern Venezuela and Venezuelan Andes.

[28] The interpolated/extrapolated map of Poisson's ratio from 34 measurements is shown in Figure 5b. We used the same algorithm except for using a grid size of 0.5° × 0.5°. Both maps show a good correlation with tectonic and

Table 2. Measured Moho Depth and V_P/V_S Ratio

Station	Lat., °	Lon., °	Elevation, km	No. RFs	H,[a] km	ϕ[b]	σ[c]	GT[d]
LUEV	5.8433	−61.4613	1.3803	28	36.5 ± 1.3	1.736 ± 0.032	0.252 ± 0.014	GS
EDPC	6.7126	−61.6392	0.1228	34	36.3 ± 1.1	1.730 ± 0.023	0.249 ± 0.010	GS
MOPC	6.5861	−66.8426	0.0957	37	37.6 ± 0.9	1.765 ± 0.019	0.249 ± 0.010	GS
CAIV	7.3262	−66.3216	0.0760	34	38.7 ± 1.0	1.783 ± 0.011	0.271 ± 0.004	GS
CAPC	7.3429	−61.8256	0.1765	36	35.0 ± 1.0	1.768 ± 0.030	0.265 ± 0.012	GS
MAPC	7.4169	−65.1881	0.0516	15	40.6 ± 1.0	1.700 ± 0.013	0.235 ± 0.006	GS
CMPC	7.6508	−64.0731	0.1427	36	38.5 ± 0.9	1.730 ± 0.014	0.249 ± 0.006	GS
GURV	7.7598	−63.0854	0.1926	34	37.5 ± 1.4	1.812 ± 0.017	0.281 ± 0.006	GS
VIPC	7.8605	−62.0655	0.2578	25	35.2 ± 1.4	1.756 ± 0.025	0.260 ± 0.010	GS
RIOV	8.0690	−61.8145	0.2320	30	35.4 ± 1.1	1.765 ± 0.012	0.264 ± 0.005	GS
PAYV	5.4205	−67.6561	0.0898	29	31.4 ± 1.2	1.810 ± 0.037	0.280 ± 0.014	GS
PAPC	8.0344	−62.6550	0.4688	24	43.8 ± 0.3	–	–	GS
SIPC	9.3596	−63.0575	0.0362	27	46.4 ± 0.3 17.4 ± 0.3[e]	–	–	FB
GUNV	10.1449	−62.9426	0.0640	34	48.4 ± 1.2	1.809 ± 0.016	0.280 ± 0.006	FB
MNPC	8.9876	−62.7444	0.0430	27	47.4 ± 0.7	–	–	FB
ORIV	9.0696	−63.4180	0.1020	4	–	–	–	FB
ARPC	9.7438	−63.7972	0.2956	17	49.8 ± 0.4	–	–	FB
PRPC	8.5019	−63.6250	0.1425	27	40.0 ± 1.0	–	–	FB
SRPC	9.5825	−64.2942	0.3202	38	49.2 ± 2.4	–	–	FB
ABPC	9.4608	−64.8207	0.1088	7	–	–	–	FB
PARV	8.9653	−64.7956	0.0206	7	52.6 ± 0.7	–	–	FB
MUPC	8.3274	−64.2946	0.1298	33	–	–	–	FB
ZUPC	8.3597	−65.1951	0.0934	27	–	–	–	FB
LAPC	8.9850	−65.7719	0.1608	21	–	–	–	FB
STPC	8.1365	−66.2544	0.0790	34	50.4 ± 1.0 25.6 ± 0.8[e]	–	–	FB
PFPC	8.3276	−65.9443	0.1312	6	48.0 ± 2.0 27.0 ± 0.9[e]	–	–	FB
RPPC	8.9485	−66.4361	0.1622	11	38.4 ± 1.5	1.783 ± 0.013	0.271 ± 0.005	FB
MERV	9.2617	−66.2972	0.1680	33	46.2 ± 1.5	–	–	FB
SMPC	8.5127	−66.3219	0.1203	30	39.4 ± 1.0	1.625 ± 0.018	0.195 ± 0.011	FB
FCPC	9.6502	−66.8342	0.2100	17	–	–	–	FB
ULPC	8.8571	−67.3865	0.1018	21	42.7 ± 1.0 22.2 ± 1.0[e]	–	–	FB
LMPC	9.3553	−67.3843	0.1459	9	–	–	–	FB
BAUV	8.9433	−68.0415	0.1060	35	42.3 ± 1.1	1.724 ± 0.009	0.246 ± 0.004	FB
ELOV	7.0011	−69.4832	0.1011	30	47.8 ± 1.3	–	–	FB
PCRV	10.1633	−64.5897	0.3950	21	31.4 ± 1.3	–	–	CP
CUPV	10.0639	−65.8056	0.6340	34	42.9 ± 1.5 20.2 ± 0.8[e]	1.708 ± 0.023	0.239 ± 0.011	CP
BIRV	10.4757	−66.2692	0.2000	19	40.0 ± 1.1	1.777 ± 0.015	0.268 ± 0.006	CP
TEST	10.4692	−66.8102	0.8750	8	–	–	–	CP
GUIV	10.6377	−62.2082	0.0500	25	28.2 ± 1.3	–	–	SI
CRUV	10.6165	−63.1842	0.6080	29	24.5 ± 0.9	1.752 ± 0.033	0.258 ± 0.014	SI
CACO	10.4782	−63.6506	0.0460	14	26.1 ± 0.6	1.829 ± 0.027	0.287 ± 0.009	SI
CARI	10.1941	−63.5301	1.1970	15	29.7 ± 0.8	1.795 ± 0.034	0.275 ± 0.013	SI
GUAY	10.6510	−63.8269	0.0110	14	28.2 ± 1.2	1.754 ± 0.033	0.259 ± 0.014	SI
CUPC	10.1576	−63.8264	1.4029	20	30.6 ± 0.8	–	–	SI
ROPC	9.9092	−66.3847	0.4325	12	23.0 ± 1.2	–	–	SI
JMPC	9.8872	−67.3968	0.4975	28	29.8 ± 1.5	–	–	SI
TURV	10.4474	−67.8382	0.2000	32	25.2 ± 2.7	1.761 ± 0.096	0.262 ± 0.044	SI
TERV	9.9586	−69.2865	1.2350	35	29.0 ± 2.0	–	–	SF
JACV	11.0866	−68.8342	0.3690	22	26.4 ± 1.1	1.818 ± 0.046	0.283 ± 0.017	SF
CURV	10.0128	−69.9611	0.7500	32	36.7 ± 1.0	1.748 ± 0.012	0.257 ± 0.005	SF
SIQV	10.6489	−69.8079	0.4000	33	37.6 ± 1.0	1.649 ± 0.014	0.209 ± 0.008	SF
QARV	10.2061	−70.5234	0.5480	7	38.4 ± 0.7	1.776 ± 0.016	0.268 ± 0.006	SF
DABV	10.9219	−70.6362	0.1469	22	31.1 ± 0.9	1.788 ± 0.020	0.272 ± 0.008	SF
SANV	9.5010	−69.5365	1.0830	4	39.1 ± 1.0	1.670 ± 0.013	0.220 ± 0.007	VA
SDV	8.8863	−70.6260	1.5800	185	52.9 ± 3.2	–	–	VA
SOCV	8.2842	−70.8566	0.3250	33	40.0 ± 1.2	1.663 ± 0.016	0.217 ± 0.009	VA
VIGV	8.8401	−71.3642	0.4300	27	51.1 ± 0.5 19.0 ± 0.8[e]	–	–	VA
CAPV	7.8649	−72.3143	1.1780	28	45.8 ± 1.60	1.730 ± 0.010	0.249 ± 0.004	VA
VIRV	10.5030	−72.4061	0.1480	34	51.0 ± 0.9	–	–	VA
ITEV	11.3552	−63.1320	−0.0061	26	23.2 ± 0.9	1.821 ± 0.024	0.284 ± 0.008	OI
COCH	10.7858	−63.9925	0.0150	16	27.3 ± 1.9	1.782 ± 0.065	0.270 ± 0.027	OI
MIPC	10.9455	−64.2944	0.0032	9	–	–	–	OI
IBAV	11.8216	−64.5977	0.0100	14	24.0 ± 2.0	–	–	OI
CURA	12.1798	−68.9592	0.0540	18	–	–	–	OI
ARUB	12.5088	−70.0009	0.0190	7	–	–	–	OI
MONV	11.9550	−69.9705	0.2390	29	26.4 ± 1.0	1.825 ± 0.021	0.285 ± 0.007	OI
IMOV	12.3585	−70.9023	0.0659	33	16.2 ± 0.4 48.8 ± 0.4[e]	–	–	OI
B151	12.9915	−67.6513	−3.6160	18	–	–	–	OB
BLOS	11.5708	−61.6677	−0.4610	22	–	–	–	OB
BTBT	11.4989	−62.5010	−0.1290	0	–	–	–	OB
CUBA	11.8499	−65.4180	−3.9970	9	19.2 ± 0.4	–	–	OB
DKSS	11.7515	−63.7699	−1.1170	12	18.5 ± 0.4	–	–	OB
DRKS	11.9992	−62.6685	−2.4000	12	–	–	–	OB

Table 2. (continued)

Station	Lat., °	Lon., °	Elevation, km	No. RFs	H,[a] km	ϕ[b]	σ[c]	GT[d]
MHTO	13.9497	−66.4910	−4.9970	27	16.8 ± 1.5	–	–	OB
PINA	10.6796	−65.2200	−1.1030	25	18.0 ± 1.6	–	–	OB
PNCH	11.2493	−66.5009	−0.9080	25	15.1 ± 2.0	–	–	OB
SHRB	11.2707	−67.3496	−1.8600	25	16.2 ± 0.6	1.932 ± 0.044	0.317 ± 0.012	OB
SOMB	12.7209	−64.9313	−3.8530	25	14.0 ± 1.5	–	–	OB
ZOMB	12.4511	−63.5522	−0.6440	11	–	–	–	OB

[a]Moho depth measured from the surface for land stations and from sea floor for the OBS stations.
[b]Vp/Vs ratio.
[c]Poisson's ratio.
[d]Geological terranes, GS: Guayana Shield; FB: Foreland basins; CP: Coastal plains; SI: Serrania del Interior; SF: Serrania del Falcon; VA: Venezuelan Andes; OI: Ocean islands; OB: OBS stations (see Figure 1 for locations).
[e]Two peaks were identified with the first value being recognized as Moho depth.

geologic terranes (Figure 6). In the following paragraphs we will divide the Moho depth and V_P/V_S ratio measurements into 8 groups and discuss the basic features of each group.

[29] **The Guayana Shield**. We observed significant differences in the nature of the crust and the crust-mantle boundary between the Precambrian Guayana shield and the other terranes. The Moho depth beneath the shield is ~37.2 km on average. There is little topographic relief across the part of the shield covered by our seismic array. The standard deviation is 2.3 km from the estimates of 12 stations and only 1.4 km if the 2 stations located at the edge of the shield (PAPC and PAYV, Figure 1) are discounted. The entire Guayana Shield is composed of four Archean and Proterozoic provinces [*Ostos et al.*, 2005], and is part of a larger shield known as the Amazonian Craton [e.g., *Neves and Cordani*, 1991]. The Archean Imataca province lies in the northern end of the shield just south of the Orinoco River. It is bounded by two Proterozoic provinces, the Pastora and Cuchivero, to the southeast and southwest, respectively. A third Proterozoic province, Roraima, lies further south of the Pastora and Cuchivero provinces (Figure 1). We found stations in the northern Archean Imataca province (RIOV, PAPC, GURV, CMPC, and MAPC) generally have about 1–2 km thicker crust than those located in the southern Proterozoic provinces (LUEV, EDPC, and CAPC, PAYV, MOPC) (Table 2, Figures 1 and 6). Thus the Moho dips slightly from south to north beneath the shield. This northward dip may reflect the southern limit of elastic flexural loading induced by complicated interactions along the Caribbean-South America plate [*Jacome et al.*, 2002; *Clark et al.*, 2006].

[30] *Schmitz et al.* [2005] obtained a crustal thickness of 37–38 km directly beneath the Orinoco River from seismic refraction measurements made along a north–south profile (NS, Figure 5) extending from the shield to the coast, in good agreement with our results. *Schmitz et al.* [2002] estimated the crust beneath the Pastora province to be 43 km along an EW refraction profile recording quarry blasts from two mines in the shield (EW, Figure 5), a value considerably greater than what we measure. Our estimated Moho depths are, however, ~6 km shallower than their observations [*Schmitz et al.*, 2002, 2005]. In general one major error source in estimating Moho depth from receiver function analysis is the assumed velocity model used in converting traveltimes to depths. This should not be the case here since we used the velocity models of *Schmitz el al.* [2002, 2005] to estimate Moho depths. Moreover, it requires an unreasonable high crustal velocity (7.4 km/s) to match our observation to their active source results. The discrepancy could also be caused by different sampling nature in active and passive seismic data as the two have very different frequency contents, and the former samples from above, while the latter samples from below. If the crust-mantle transition is a gradient boundary, the estimated Moho depth depends on the wavelength used to measure it. While high frequency active source data more or less report the depth associated with a rapid change in velocity, the long wavelength teleseismic waves are likely to give the average depth of the whole transition. The two could be different from each other depending on the fine structure of the crust-mantle transition. However, as we discuss below the observed receiver functions suggested that the Moho must be a sharp boundary with a thickness of less than 2 km, making this argument unlikely. The quarry blast data were sampled with receivers on average spaced at about 7 km apart. There were no Pn or Sn observations, Moho depths were solely determined from arrival times of PmP, resulting in a large uncertainty in the estimated crustal thickness. The Moho thickness is thus not well determined beneath the Pastora province. We note that the *Schmitz et al.* [2005] refraction results, from a survey utilizing controlled shots, agrees well with our results at the northernmost edge of the craton. We suggest that the phase correlations in the poorly sampled quarry blast data may be misidentified, or the ripple fired blasts have produced signals that have led to inconsistent traveltime picks at near and far distance.

[31] Another distinct feature shown in the receiver functions from the craton is the large amplitude P to S converted waves as well as the strong crustal reverberation phases (Figures 3 and 4a). This indicates that the Moho beneath each station must be very flat and have a large change in velocity and density across it. The crust-mantle boundary must be sharp with a transition zone less than a few kilometers. The reverberation phases 2p1s and 1p2s exhibit waveform broadening compared to the direct P wave (Figure 4a). We used a forward modeling approach [*Niu and James*, 2002] to estimate the upper boundary of the thickness of the crust-mantle transition. If the observed broadening is caused entirely by a velocity gradient across the Moho, then the width of the waveform of 1p2s constrains the allowable extent of the transition zone to be less than 2 km.

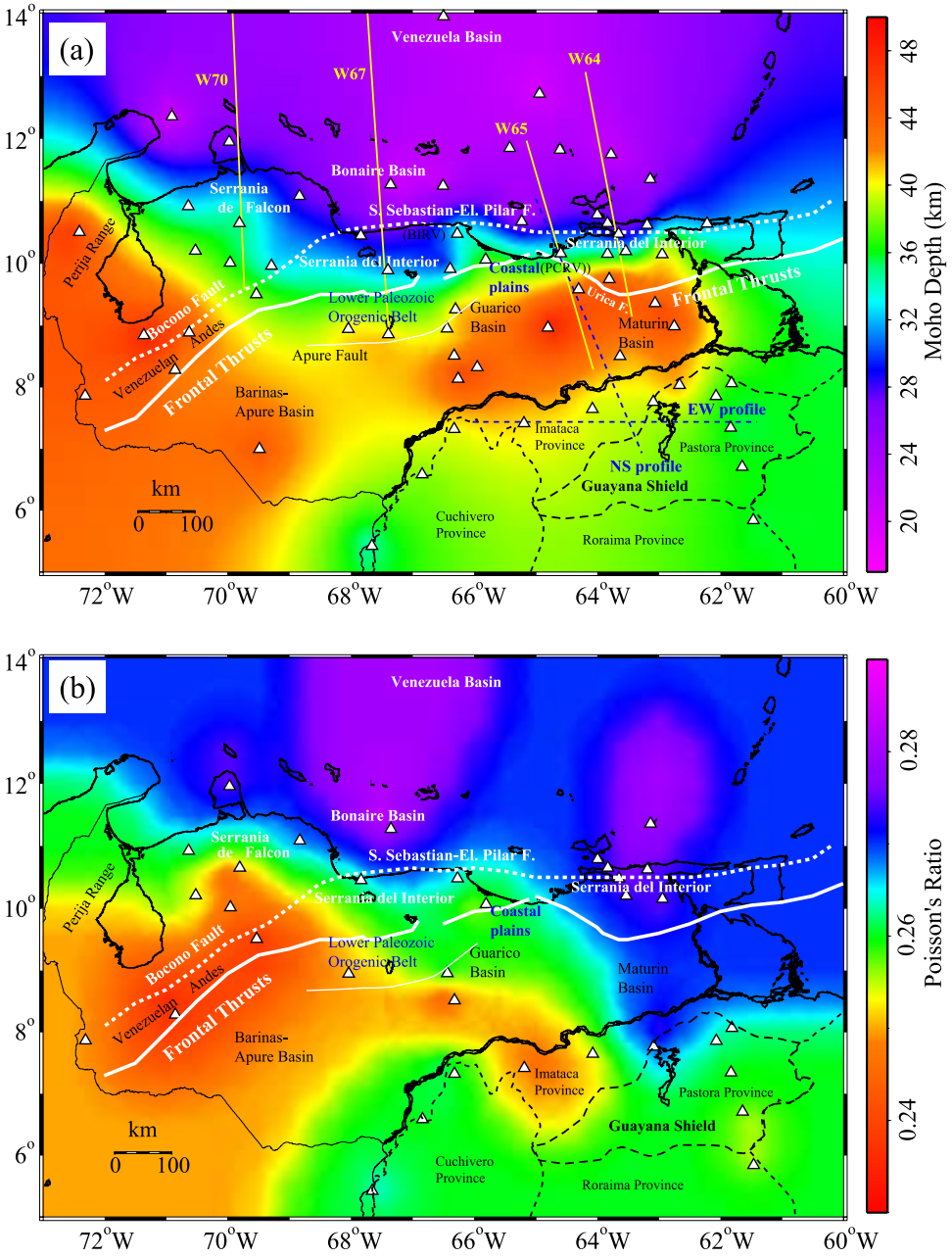

Figure 5. Maps showing the Moho relief (a) and variations of the Poisson's ratio (b). The color contour is based on the observations at stations shown as white triangles. Interpolation was performed to minimize the lateral variations of Moho depth and Poisson's ratio (see text for details). The corners of the map are poorly constrained. Major fault systems are shown as white lines, with the dotted and solid lines indicate strike-slip and thrust faults, respectively. The reflection/wide-angle profiles of the BOLVIVAR project that we used to derive our reference models are shown as yellow lines labeled by W70, W67, W65 and W64. Locations of the active source refraction profiles of *Schmitz et al.* [2002, 2005] are indicated by dashed blue lines labeled as EW and NS profiles.

[32] In principle, it is also possible to model changes in V_S and density with the amplitude information of the P to S conversion phases and the two reverberation phases [*Niu and James*, 2002]. We found, however, the uncertainty is still too large to give valuable constraints on the velocity and density in the lowermost crust. We obtained 11 estimates of the V_P/V_S ratio from the 12 stations (Figure 7). The average ratio is 1.760, which is equivalent to an average Poisson's ratio (σ_a) of 0.262. σ_a does not appear to have any obvious dependence on geologic age within the Precambrian terranes. Four of the five stations with the highest σ_a are found along the Orinoco River near the border between the craton and foreland basins (Table 2, Figure 1).

[33] The observed σ_a value (0.262) is almost the same as the continental crustal average (0.265) [*Christensen and Mooney*, 1995]. In a global study, *Zandt and Ammon* [1995]

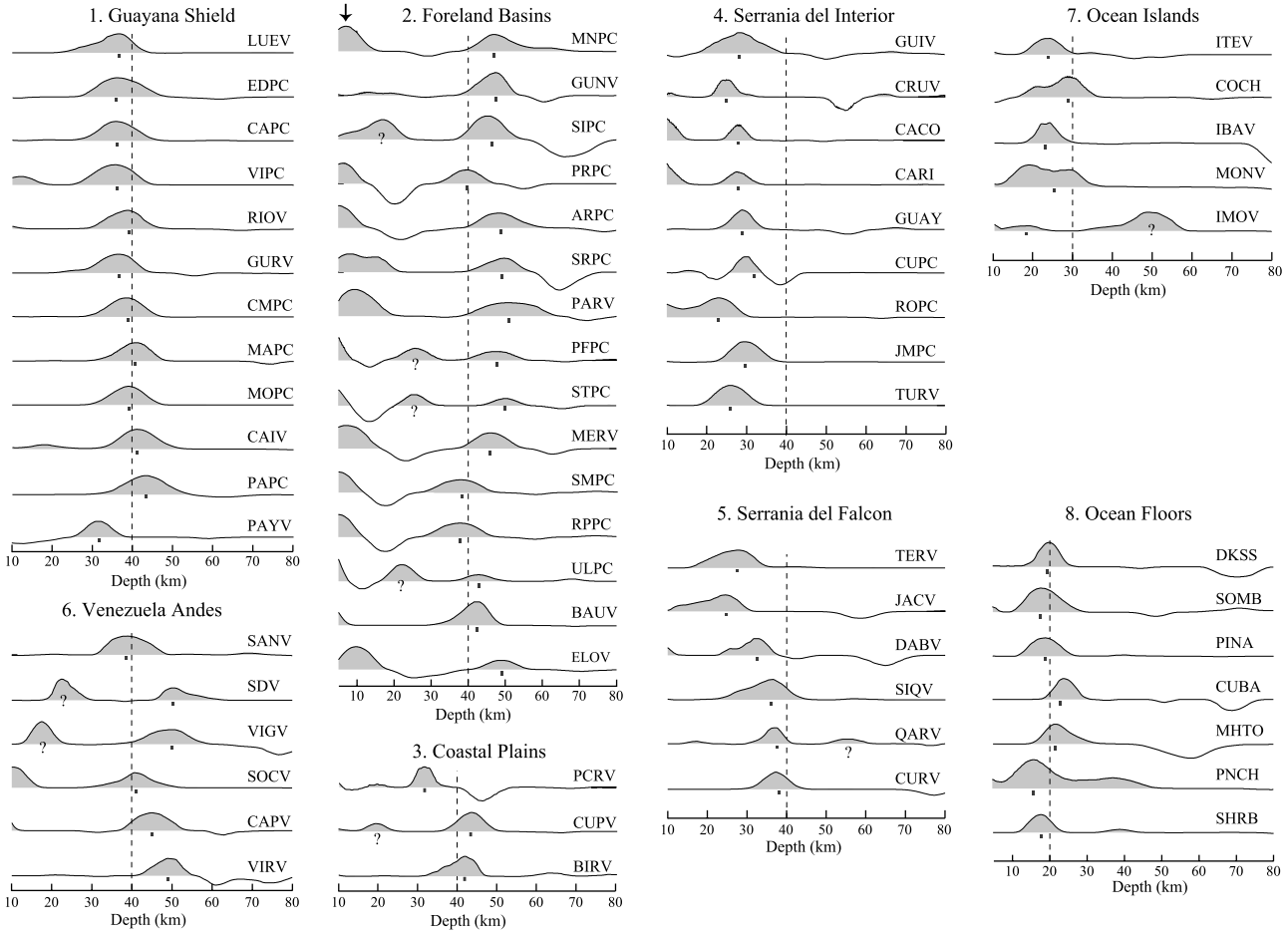

Figure 6. Stacked receiver functions sorted by tectonic terranes: 1. Guayana Shield; 2. Foreland basins; 3. Coastal plains; 4. Serrania del Interior; 5. Serrania del Falcon; 6. Venezuelan Andes; 7. Ocean islands; 8. Ocean floors. Reference line of 40 km for land stations, 30 km for ocean islands, and 10 km for ocean floor stations. Arrow indicates the base of the sedimentary layer observed mainly from the stations in the foreland basins. Square dots indicate the identified Moho depth. Traces with question marks show two peaks and our identifications are based solely on the consistency with other stations and thus could be arbitrary.

concluded that the crust of ancient shields is characterized by a relatively high Poisson's ratio (0.29), which is indicative of mafic material in the lowermost crust. For the Guayana Shield studied here, however, the measured σ_a indicate that it can accommodate only relatively small amounts of granulite-facies mafic components. The lack of a high velocity mafic layer is indirectly supported by the large velocity contrast across the Moho inferred from the large amplitude of conversion and reverberation phases. The results here are consistent with observations in South Africa [*Niu and James*, 2002] and west Australia [*Durrheim and Mooney*, 1994]. However, we could not identify a difference in lower crustal structure between the Archean and Proterozoic crust as suggested by *Durrheim and Mooney* [1994].

[34] **The Foreland Basins**. This region consists of the Barinas-Apure Basin, Guarico Basin and Maturin Basin located at the south side of the Frontal Thrusts (Figures 1 and 5). The region between Guarico and Barinas-Apure basin is a former Paleozoic orogenic belt that has been eroded [*Ostos et al.*, 2005]. The Maturin and Guarico basins are relatively well instrumented compared to the Barinas-Apure Basin in the west mainly because of annual flooding during the wet season. In general the quality of the receiver functions recorded in basins is poor due to the low similarity between the horizontal and vertical components of the recordings. This is probably due to the strong sediment-induced reverberations. We were able to obtain 15 depth measurements from a total of 22 stations deployed in this region (Table 2, Figures 1 and 6). The average crustal Moho depth is 45.8. There is a large conversion at depths between 4 and 15 km which we interpret as the base of the sediment layer, as we used the P-SV pair in the receiver function analysis and the P wave energy should be minimized in the receiver functions. The thickest crust is observed in the eastern Maturin basin where very large Bouguer gravity anomalies (−160 mGal) and an extremely thick sedimentary column (>10 km) have been observed previously [*Schmitz et al.*, 2005]. The crust beneath the Guarico Basin and the Paleozoic orogenic belt appears to be shallower than that of the Maturin Basin. We suggest that the shallower Moho depth might result from the lack of thrust loading, or continental subduction, or both along the coast here. We

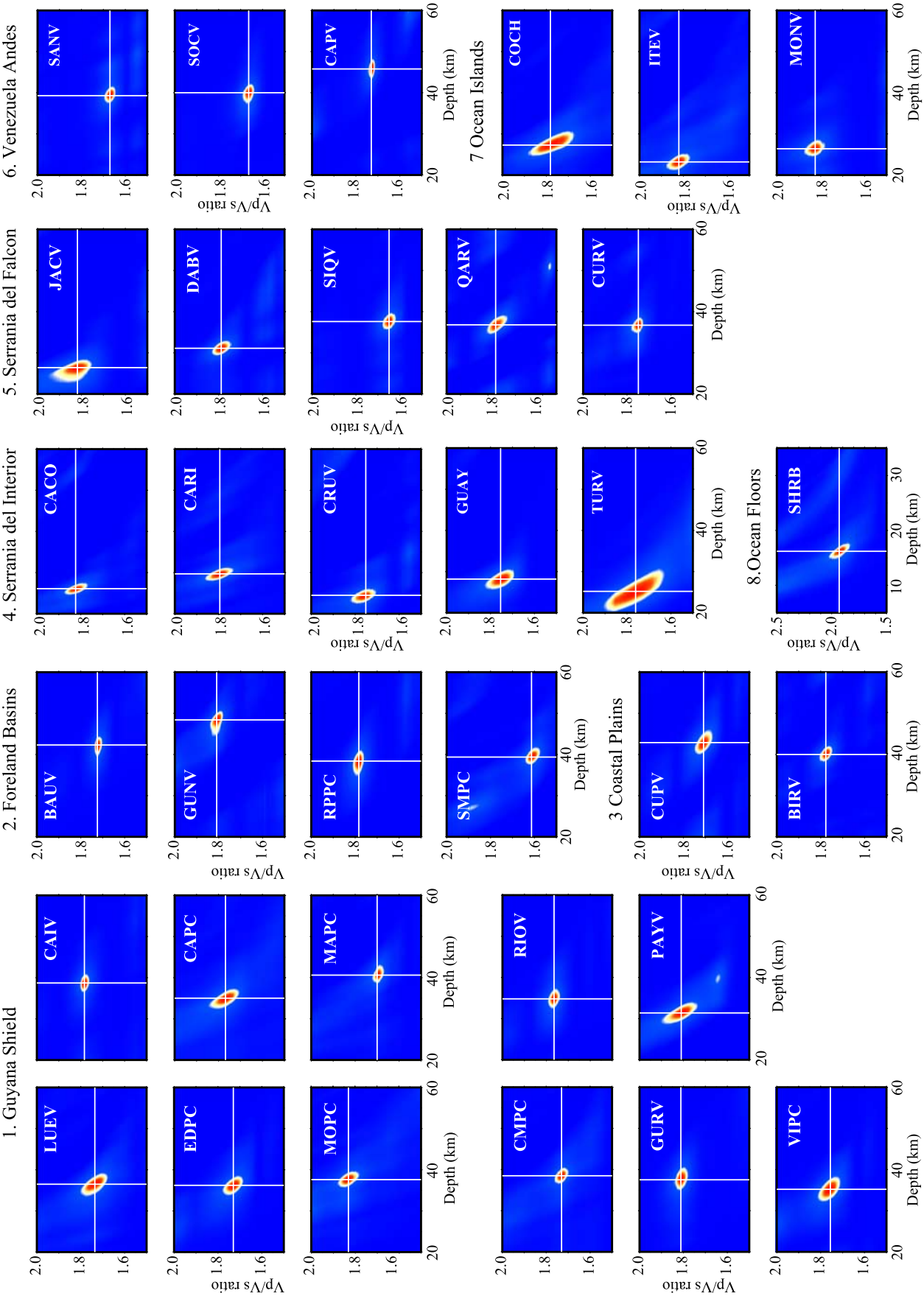

Figure 7. Moho depth and V_P/V_S ratio measurements. Color scaling is similar to Figure 4b. The best depth and ratio is indicated by the two white lines.

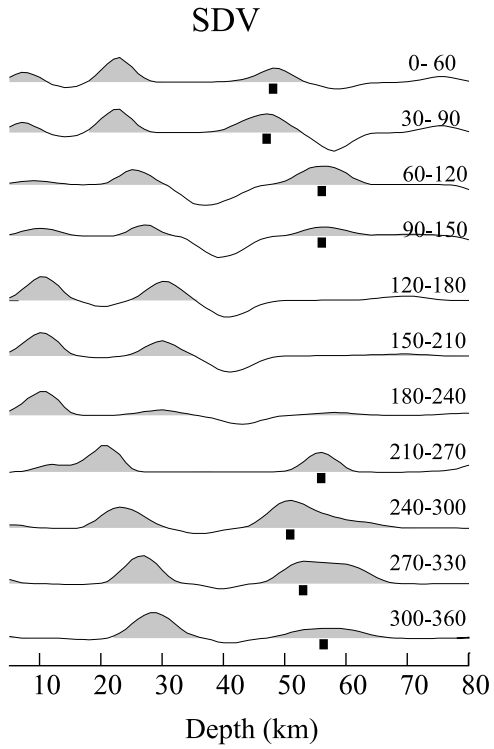

Figure 8. Depth stacked receiver functions gathered at 11 back azimuth bins. Numbers above each trace indicate the back azimuth ranges. The SV receiver functions recorded at station SDV are displayed.

also found that the crust beneath the Guarico Basin and the Paleozoic orogenic belt is more complex. Several stations in this area show two prominent P to S conversion peaks of which we picked the deeper one in order to keep the Moho as flat as possible. The shallower peak we see in the old Paleozoic orogenic belt might be related to detachments or thrust faults. We obtained 4 V_P/V_S ratio measurements, with an average value of 1.735 or a Poisson's ratio of 0.248 (Figure 7). Station GUNV at the northeastern edge of the Maturin basin has the largest ratio, while the three stations at the edge of the Paleozoic orogenic belt (RPPC, SMPC and BAUV) appear to have low Poisson's ratios (Table 2, Figure 5b).

[35] **The Coastal Plains**. Here we refer to the coastal plains as the relatively flat area between the eastern and western mountain ranges of the Serrania del Interior. It is bounded by two towns, Puerto La Cruz (station PCRV) in the east and Birongo (station BIRV) in the west. The region is characterized by very distinct crustal thickness and V_P/V_S ratio from the coastal mountain ranges. The crust is about 37.7 km thick (Table 2, Figure 6) with a Poisson's ratio of 0.254 (Table 2, Figure 7). We also observed a shallower peak at the station CUPV, which might be related to the detachment of the nearby thrust fault (Figure 1).

[36] **The Serrania del Interior**. The Moho beneath this geological province is surprisingly flat and shallow (Figure 6). The average Moho depth is 26.8 km with a standard deviation of 2.5 km. Given that this region is characterized by an average elevation of 800 m, the mountains in this region are not isostatically balanced. This indicates that these mountains must be dynamically supported, probably from flexural rebound of the South America plate. It has been suggested that the subducted Atlantic slab has been detaching from the South America continent progressively from west to east beneath northeastern Venezuela [*VanDecar et al.*, 2003]. The tear-off could result in an upward rebound of the deflected South America plate. A more quantitative synthesis of the regional tectonics from the active and passive source data as well as numerical modeling are presented elsewhere.

[37] The relative simplicity of the crustal structure has resulted in robust measurements of σ_a (Figure 7). In general the region has a $\sigma_a = 0.268$, in good agreement with either that of average continental crust, 0.265 [*Christensen and Mooney*, 1995] or the 0.27 of *Miller and Christensen* [1994] measured on rocks from the Kohistan arc in northern Pakistan, The local σ_a thus agrees with a scenario that a large amount of the crust in this region may have an island arc origin.

[38] **The Serrania del Falcon**. We have a total of 6 stations deployed in the Tertiary Falcon Basin. Formation of this region involved uplift that started from a tectonic inversion of a marine basin resulting from NW–SE compression in the Miocene [*Audemard*, 2001] associated with the northward escape of the Maracaibo block. The 6 stations can be roughly divided into two groups. The three stations in the eastern and northern part of the basin (TERV, JACV and DABV) showed a relative thin crust around 28 km with a high Poisson's ratio of 0.278, while the crust in the central and southern areas (SIQV, QARV and CURV) has a moderate thickness of 37 km with a lower Poisson's ratio of 0.245. The average elevation of the eastern and northern stations is about 600 m above the sea level. It is thus likely that the excess topography here also has a dynamic origin. A possible source is the positive buoyancy of the Caribbean oceanic plateau thrust underneath the Falcon region [*van der Hilst and Mann*, 1994; *Guédez*, 2007].

[39] **The Venezuelan Andes**. We observed a very thick crust beneath the NE–SW trending Venezuelan Andes. The average crustal thickness is around 46 km (Table 2, Figures 5 and 6). The central part of the chain has the thickest crust which reaches ~52 km depth. The Moho shallows more rapidly toward the northeast than to the southwest, consistent with shortening related to the compression between the Maracaibo block and South America [*Audemard and Audemard*, 2002]. The crust beneath the station located in the Perija Range (VIRV) is also close to 50 km thick, indicating that both the Venezuelan Andes and the Perija Range are underlain by thick crustal roots. On the other hand we obtained very low Poisson's ratios from three stations in the Venezuelan Andes. The average Poisson's ratio is 0.229, suggesting considerably more felsic crust than the rest of Venezuela.

[40] We collected 185 receiver functions at the GSN station SDV, which lies on the southern flank of the central Venezuelan Andes. The large number of receiver functions allowed us to examine azimuthal dependence of crustal structure. We sorted the receiver functions based on the back azimuth. The stacked receiver functions gathered at 11 back azimuth bins are shown in Figure 8. In general there are two P to S conversion peaks in the stacked receiver functions and we interpreted the deeper one as the Moho in

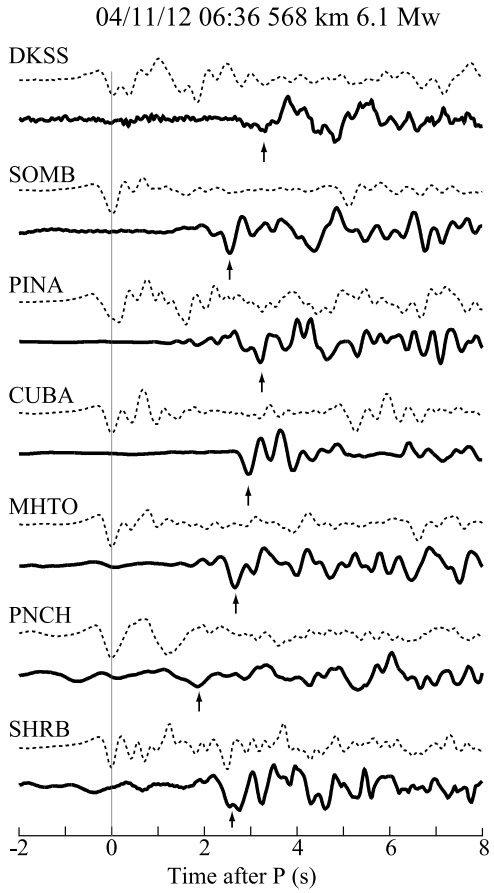

Figure 9. The vertical and radial component seismograms recorded at 7 OBS stations from a deep earthquake are shown in dashed and solid lines, respectively. Arrows indicate the Moho P to S conversions. The data are filtered with a 2s high-pass filter.

this area. We found very large variations among these back azimuth stacks. The Moho is totally absent in the receiver functions stacked from three southeastern back azimuth bins. This may be caused by a dipping Moho structure. If the Moho dips toward the northwest, teleseismic P waves arriving from southeast directions arrive at almost normal incidence to the Moho, resulting in very small P to S conversions.

[41] **The Ocean Islands**. We have broadband data from 9 islands within the Caribbean-South America plate boundary. The island stations are generally very noisy and we obtained only 5 Moho depth estimates (Table 2, Figure 6) and 3 V_P/V_S ratio measurements (Figure 7). We observed two strong P to S conversion peaks at depths of 16.2 km and 48.8 km beneath the Los Monjes Island (IMOV), the western end of the island chain. We picked the shallower one in order to keep the Moho as flat as possible although the second peak has larger amplitude. Crustal thicknesses observed at the other 4 stations have very small variations with an average thickness of 25.1 km. Both Monte Cano (MONV) and Los Testigos (ITEV) have high Poisson's ratio (0.285 and 0.284), consistent with a mafic island arc origin. Coche Island, which is located between Margarita Island and the Araya Peninsula, has a lower σ that is close to the continental average.

[42] **The Southeastern Caribbean Sea**. The Caribbean plate has long been interpreted as a large igneous plateau (LIP) with anomalously thick crust in many areas [*Case et al.*, 1990]. Through the deployment of OBSIP broadband stations, we obtained some high quality data. From one deep event (04/11/12 06:36 568 km 6.1 Mw) and one intermediate depth event (04/10/08 15:28 101 km 5.8 Mw) we were able to confirm the P to S conversions at the Moho from the radial component even before the deconvolution (Figure 9). The Moho depth obtained from the 7 OBS stations ranges from 16.0 ± 2.0 to 23.2 ± 0.4 km below sea level (Table 2, Figure 6). The thickest crust is observed beneath the Southern Caribbean Deformed Belt at station CUBA. We were able to measure the V_P/V_S ratio from one station deployed in the Bonaire Basin (SHRB, Figure 7). The observed V_P/V_S ratio is 1.932, translating to a Poisson's ratio of 0.317. The observed value here is slightly higher than the laboratory measurements for the major oceanic crustal constituents, basalt (0.294), diabase (0.279) and gabbro (0.295) at 600 MPa pressure conditions [*Christensen*, 1996]. In general, the presence of thick marine sediments and high pore fluid pressure can increase Poisson's ratio, which is a likely scenario for the Bonaire Basin, a Tertiary basin formed roughly at the same time as the now inverted Falcon Basin.

6. Conclusions

[43] The BOLIVAR array data have made it possible for us to develop a map of crustal thickness and Poisson's ratio in the complicated southeastern Caribbean plate boundary zone, and the adjacent Guayana shield. The primary results of our receiver function analysis revealed the following features of the crust and crust-mantle boundary beneath the array: (1) Moho depth in this diffuse plate boundary region is highly variable ranging from ~16 km beneath the Caribbean LIP, to ~52 km beneath eastern Venezuela; (2) crustal thickness is strongly correlated with geologic terranes, but not always as expected; (3) the crust beneath the Precambrian Guayana shield is fairly uniform with an intermediate composition and a moderate thickness of ~37 km. The Moho under the craton appears to be a sharp and flat boundary with large impedance contrasts. There is no evidence for the presence of a high velocity mafic layer in the lowermost crust under the craton; (4) the Maturin Basin is underlain by a thick crust that dips to the north, direct evidence for overthrust loading or continental subduction or both along the northern margin of the Venezuelan mainland. In contrast crust beneath the Guarico Basin and the Paleozoic orogenic belt appears to be shallower and also more complicated; (5) the measured V_P/V_S ratio from Serrania del Interior and northern Falcon suggested that they may be composed of accreted oceanic arcs. We also find a relatively thin (~25–30 km) crust beneath the two coastal mountain range systems, suggesting that a significant portion of the high topography has dynamic origins. (6) The topography of the Venezuelan (Merida) Andes and the Perija Range, on the other hand, are mainly achieved by Airy isostasy.

[44] **Acknowledgments.** We thank FUNVISIS for providing access to their new digital broadband data as part of this collaboration. We are indebted to the IRIS-PASSCAL program, a facilities program of the National Science Foundation, for providing instrumentation and technical support for this experiment. We also thank the NSF funded US National Ocean Bottom Seismograph Instrument Pool, and in particular the UCSD L-cheapo group for their support of the passive OBS deployment. We thank all the people involved in the BOLIVAR and GEODINOS projects. We owe a special debt of thanks to a long list of personnel at FUNVISIS who assisted in the PASSCAL deployment. At the Meteorological Service Netherlands Antilles & Aruba, special thanks are due to Albert Martis, Arthur Dania, and Marck Oduber for their generous support in siting, constructing and maintaining our stations in their facilities. Discussions with Hans Ave Lallemant, Stoney Clark, Cin-Ty A. Lee, Michael Schmitz and Colin Zelt were helpful in preparing the manuscript. The Associate Editor, Dr. Martha Savage and one anonymous reviewer provided very constructive reviews that improved the manuscript significantly. The BOLIVAR project is funded by the National Science Foundation Continental Dynamics Program (EAR-0222270). F.N. expresses special thanks to Rice University for the generous support for his field work.

References

Ammon, C. J. (1991), The isolation of receiver effects from teleseismic P waveforms, *Bull. Seismol. Soc. Am.*, *81*, 2504–2510.

Aster, R., B. Borchers, and C. Thurber (2004), *Parameter Estimation and Inverse Problems*, *Int. Geophys. Ser.*, vol. 90, 301 pp., Elsevier, New York.

Audemard, F. A. (2001), Quaternary tectonics and present stress tensor of the inverted northern Falcon Basin, northwestern Venezuela, *J. Struct. Geol.*, *23*, 431–453.

Audemard, F. E., and F. A. Audemard (2002), Structure of the Merida Andes, Venezuela: Relations with the South America-Caribbean geodynamic interaction, *Tectonophysics*, *345*, 299–327.

Burke, K. (1988), Tectonic evolution of the Caribbean, *Ann. Rev. Earth Planet. Sci.*, *16*, 201–230.

Case, J. E., W. MacDonald, and P. J. Fox (1990), Caribbean crustal provinces, seismic and gravity, in *The Caribbean Region*, G. Dengo and J. E. Case (Eds.), Geological Soc. of America, Boulder Colorado, pp.15–36.

Christensen, N. I. (1996), Poisson's ratio and crustal seismology, *J. Geophys. Res.*, *101*, 3139–3156.

Christensen, N. I., and W. D. Mooney (1995), Seismic velocity structure and composition of the continental crust: A global view, *J. Geophys. Res.*, *100*, 9761–9788.

Clark, S. A., F. Niu, A. Levander, and the BOLIVAR Working Group (2006), Tearing the lithosphere: Diachronous slab detachment along the Venezuelan margin from BOLIVAR seismic data, *Eos Trans. AGU*, *87*(52), Fall Meet. Suppl., Abstract, T42C-06.

Clayton, R. W., and R. A. Wiggins (1976), Source shape estimation and deconvolution of teleseismic body waves, *Geophys. J. R. Astron. Soc.*, *47*, 151–177.

de Wit, M. D., C. E. J. de Ronde, M. Tredoux, C. Roering, R. J. Hart, R. A. Armstrong, R. W. E. Green, E. Peberdy, and R. A. Hart (1992), Formation of an Archaean continent, *Nature*, *357*, 553–562.

Dueker, K. G., and A. F. Sheehan (1998), Mantle discontinuity structure beneath the Colorado Rocky Mountains and High Plains, *J. Geophys. Res.*, *103*, 7153–7169.

Durrheim, R. J., and W. D. Mooney (1994), Evolution of the Precambrian lithosphere: Seismological and geochemical constraints, *J. Geophys. Res.*, *99*, 15,359–15,374.

Efron, B., and R. Tibshirani (1986), Bootstrap methods for standard errors, confidence intervals, and other measures of statistical accuracy, *Stat. Sci.*, *1*, 54–75.

Fountain, D. M., and N. I. Christensen (1989), Composition of the continental crust and upper mantle: a review, in *Geophysical Framework of the Continental United States*, L. C. Pakiser and W. D. Mooney (Eds.), Geol. Soc. Am. Mem. 172, Boulder, CO, pp.711–742.

Gordon, R. G. (1998), The plate tectonic approximation: Plate non rigidity, diffuse plate boundaries, and global plate reconstructions, *Ann. Rev. Earth Planet. Sci.*, *26*, 615–642.

Guédez, M. C. (2007), BOLIVAR: Crustal Structure across the Caribbean-South American Plate Boundary at 70W- Results from Seismic Refraction and Reflection Data, M.S. Thesis, Rice Univ., Houston, TX, USA, 41 pp.

Guédez, M. C., C. A. Zelt, M. B. Magnani, and A. Levander (2006), BOLIVAR: Crustal structure of the Caribbean-South America plate boundary at 70W, *EOS, Trans AGU*, Abstract T43D-1677.

Gurrola, H., J. B. Minster, and T. Owens (1994), The use of velocity spectrum for stacking receiver functions and imaging upper mantle discontinuities, *Geophys. J. Int.*, *117*, 427–440.

Gurrola, H., G. E. Baker, and J. B. Minster (1995), Simultaneous time-domain deconvolution with application to the computation of receiver function, *Geophys. J. Int.*, *120*, 537–543.

Henstock, T. J., A. Levander, and the Deep Probe Working Group (1998), Probing the Archean and Proterozoic lithosphere of western North America, *GSA Today*, *8*, 1–5, 16–17.

Hoffman, P. F. (1988), United plates of America, the birth of a craton: Early Proterozoic assembly and growth of Laurentia, *Ann. Rev. Earth Planet. Sci.*, *16*, 543–603.

Holbrook, W. S., D. Lizarralde, S. McGeary, N. Bangs, and J. Diebold (1999), Structure and composition of the Aleutian island arc and implications for continental crustal growth, *Geology*, *27*, 31–34.

Jacome, M. I., N. Kusznir, F. Audemard, and S. Flint (2002), The Formation of the Maturin Foreland Basin, Eastern Venezuela: Thrust Sheet Loading or Subduction Dynamic Topography, *Tectonics*, *22*(5), 1046, doi:10.1029/2002TC001381.

Jordan, T. H. (1988), Structure and formation of the continental tectosphere, *J. Petrology*, Special Lithospher Issue, 11–37.

Kanasewich, E. R. (1973), *Time Sequence Analysis in Geophysics*, Univ. of Alberta Press, Edmonton, AB, pp. 364.

Langston, C. A. (1979), Structure under Mount Rainier, Washington, inferred from teleseismic body waves, *J. Geophys. Res.*, *84*, 4749–4762.

Levander, A. (2003), USArray design implications for wavefield imaging in the lithosphere and upper mantle, *The Leading Edge*, *22*, 250–255.

Levander, A., et al. (2006), Evolution of the Southern Caribbean plate boundary, *Eos Trans. AGU 87*, *97*, 2006.

Miller, D. J., and N. I. Christensen (1994), Seismic signature and geochemistry of an island arc: A multidisciplinary study of the Kohistan accreted terrane, northern Pakistan, *J. Geophys. Res.*, *99*, 11,623–11,642.

Mooney, W. D., G. Laske, and G. Masters (1998), CRUST 5.1: A global crustal model at $5^\circ \times 5^\circ$, *J. Geophys. Res.*, *103*, 727–747.

Muirhead, K. J. (1968), Eliminating false alarms when detecting seismic events automatically, *Nature*, *217*, 533–534.

Nelson, K. D. (1991), A unified view of craton evolution motivated by recent deep seismic reflection and refraction results, *Geophys. J. Int.*, *105*, 25–35.

Neves, B. B., and U. G. Cordani (1991), Tectonic evolution of South America during the Late Proterozoic, *Precambrian Res.*, *53*, 23–40.

Nguuri, T. K., J. Gore, D. E. James, S. J. Webb, C. Wright, T. G. Zengeni, O. Gwavana, and J. A. Snoke (2001), Kaapvaal Seismic Group, Crustal structure beneath southern Africa and its implications for the formation and evolution of the Kaapvaal and Zimbabwe cratons, *Geophys. Res. Lett.*, *28*, 2501–2504.

Niu, F., and D. E. James (2002), Fine structure of the lowermost crust beneath the Kaapvaal craton and its implications for crustal formation and evolution, *Earth Planet. Sci. Lett.*, *200*, 121–130.

Niu, F., and H. Kawakatsu (1996), Complex structure of the mantle discontinuities at the tip of the subducting slab beneath the northeast China: A preliminary investigation of broadband receiver functions, *J. Phys. Earth*, *44*, 701–711.

Niu, F., and H. Kawakatsu (1998), Determination of the absolute depths of the mantle transition zone discontinuities beneath China: Effect of stagnant slabs on mantle transition zone discontinuities, *Earth Planets Space*, *50*, 965–975.

Niu, F., A. Levander, C. M. Cooper, C.-T. Aeolus Lee, A. Lenardic, and D. E. James (2004), Seismic constraints on the depth and composition of the mantle keel beneath the Kaapvaal craton, *Earth Planet. Sci. Lett.*, *224*, 337–346.

Ostos, M., F. Yoris, and H. G. Ave Lallemant (2005), Overview of the southeast Caribbean-South America plate boundary zone, in: *Caribbean-South American Plate Interactions, Venezuela*, H. G. Ave Lallemant and V. B. Sisson (Eds.), Geol. Soc. Am. Special Paper 394, Boulder CO, pp.53–89.

Owens, T. J., G. Zandt, and S. R. Taylor (1984), Seismic evidence for an ancient rift beneath the Cumberland plateau, Tennessee: A detailed analysis of broadband teleseismic P waveforms, *J. Geophys. Res.*, *89*, 7783–7795.

Park, J., and V. Levin (2000), Receiver functions from multiple-taper spectral correlation estimates, *Bull. Seismol. Soc. Am.*, *90*, 1507–1520.

Poppeliers, C., and G. Pavlis (2003), Three-dimensional, prestack, plane wave migration of teleseismic P-to-S converted phases: 1. Theory, *J. Geophys. Res.*, *108*(B2), 2112, doi:10.1029/2001JB000216.

Reading, A., B. L. N. Kennett, and M. Sambridge (2003), Improved inversion for seismic structure using transformed, S-wave vector receiver functions: Removing the effect of the free surface, *Geophys. Res. Lett.*, *30*(19), 1981, doi:10.1029/2003GL018090.

Rudnick, R. L., and D. M. Fountain (1995), Nature and composition of the continental crust: A lower crustal perspective, *Rev. Geophys.*, *33*, 267–309.

Schmitz, M., D. Chalbaud, J. Castillo, and C. Izarra (2002), The crustal structure of the Guayana Shield, Venezuela, from seismic refraction and gravity data, *Tectonophysics*, *345*, 103–118.

Schmitz, M., A. Martins, C. Izarra, M. I. Jacome, J. Sanchez, and V. Rocabado (2005), The major features of the crustal structure in northeastern Venezuela from deep wide-angle seismic observations and gravity modelling, *Tectonophysics*, *399*, 109–204.

Sheehan, A. F., P. M. Shearer, H. J. Gilbert, and K. G. Dueker (2000), Seismic migration processing of P–SV converted phases for mantle discontinuity structure beneath the Snake River Plain, western United States, *J. Geophys. Res.*, *105*, 19,055–19,065.

Snelson, C. M., T. J. Henstock, G. R. Keller, K. C. Miller, and A. Levander (1998), Crustal and uppermost mantle structure along the Deep Probe seismic profile, *Rocky Mountain Geology*, *33*, 181–198.

Suyehiro, K., N. Takahashi, Y. Ariie, Y. Yokoi, R. Hino, M. Shinohara, T. Kanazawa, N. Hirata, H. Tokuyama, and A. Taira (1996), Continental crust, crustal underplating, and Low-Q upper mantle beneath an oceanic island arc, *Science*, *272*, 390–392.

Taylor, S. R. (1967), The origin and growth of continents, *Tectonophysics*, *4*, 17–34.

Taylor, S. R., and S. M. McLennan (1985), *The continental Crust: its Composition and Evolution: An Examination of the Geochemical Record Preserved in Sedimentary Rocks (GT)*, Blackwell Publishing Ltd, Oxford, UK.

Taylor, S. R., and A. R. White (1965), Geochemistry of andesites and the growth of continents, *Nature*, *208*, 271–273.

VanDecar, J. C., R. M. Russo, D. E. James, W. B. Ambeh, and M. Franke (2003), Aseismic continuation of the Lesser Antilles slab beneath continental South America, *J. Geophys. Res.*, *108*(B1), 2043, doi:10.1029/2001JB000884.

Van der Hilst, R. D., and P. Mann (1994), Tectonic implications of tomographic images of subducted lithosphere beneath northwestern South America, *Geology*, *22*, 451–454.

Vinnik, L. P. (1977), Detection of waves converted from P to SV in the mantle, *Phys. Earth Planet. Inter.*, *15*, 39–45.

Yilmaz, O. (2001), Seismic Data Analysis: Processing, Inversion and Interpretation of Seismic Data, *Soc. of Explor. Geophys.*, Tulsa, OK.

Zandt, G., and C. J. Ammon (1995), Continental crust composition constrained by measurement of crustal Poisson's ratio, *Nature*, *374*, 152–154.

Zhu, L., and H. Kanamori (2000), Moho depth variation in southern California from teleseismic receiver functions, *J. Geophys. Res.*, *105*, 2969–2980.

M. Bezada, A. Levander, and F. Niu, Department of Earth Science, Rice University, 6100 Main Street, Houston, TX 77005, USA. (niu@rice.edu)

T. Bravo and G. Pavlis, Department of Geological Sciences, Indiana University, USA.

H. Rendon, FUNVISIS, El Llanito, Venezuela.

F. Vernon, Scripps Institution of Oceanography, University of California, USA.